

Quantum annealing in a disordered Ising chain with tuned inhomogeneous transverse field

Tatsuhiko Shirai^{1*} and Shu Tanaka^{2,3†}

¹*Department of Computer Science and Communications Engineering,
Waseda University 3-4-1, Ookubo,
Shinjuku-ku, Tokyo, 169-8555 Japan*

²*Department of Applied Physics and Physico-Informatics,
Keio University, 3-14-1, Hiyoshi,
Kohoku-ku, Yokohama, 223-8522, Japan
and*

³*Green Computing System Research Organization,
Waseda University, Wasedamachi-27,
Shinjuku-ku, Tokyo, 162-0042, Japan*

We investigate the effect of tuned inhomogeneous transverse field in a disordered Ising chain on properties of the quantum phase transition and performance of quantum annealing. We set the strength of the transverse field on a spin in proportion to the coupling strength connecting the spin. This setting of transverse field gives a qualitative difference from previous studies, where the transverse field is homogeneous over spins or random independently of the coupling strength. We find that the dynamical critical exponent is finite in contrast to previous studies where it is infinity. We numerically confirm that the performance of quantum annealing is improved as expected from the Kibble–Zurek mechanism. This work demonstrates an importance of tuning the transverse field on each spin in quantum annealing.

I. INTRODUCTION

Quantum annealing (QA) is a metaheuristic algorithm to find the ground state of a random Ising model with the aid of the effect of quantum fluctuations [1, 2]. In the algorithm, the system is initially prepared in the ground state of the Hamiltonian of transverse field, and evolves in time under the Hamiltonian which is continuously deformed into the one of the random Ising model. The adiabatic theorem of quantum mechanics [3] guarantees that the system will reach the ground state of the random Ising model if the rate of the deforming is sufficiently small compared to the energy gap between the ground state and the first excited state. When a quantum phase transition (QPT) [4] exists during QA, the performance of QA is dominantly determined by the properties of QPT because the gap is closing at the transition point. At the first-order (discontinuous) QPT point, the gap decays exponentially with the system size, which implies that it takes an exponentially long time to obtain the ground state [5]. There have been efforts to avoid the first-order QPTs [6–10]. At the second-order (continuous) QPT, the gap usually exhibits a power-law decay with the system size. The performance of QA is given by the critical exponents characterizing the diverging time scale and the diverging length scale. This is called the Kibble–Zurek mechanism (KZM) [11, 12], and has been

discussed in theory [13–15] (for reviews see [16, 17]) and in experiments [18–21] (for a review see [22]).

A disordered Ising chain with a transverse field is one of the prototypical models for studying the relation between the properties of the QPT and the performance of the QA. The nearest-neighbor coupling strength is randomly distributed and assumed to be ferromagnetic without loss of generality. The transverse field has been set to be homogeneous over spins [23] or randomly chosen independently of the nearest-neighbor coupling strength [24, 25]. In both cases, qualitatively the same results have been reported. As the transverse field is decreasing, the system shows a continuous QPT from a paramagnetic phase to an ordered phase. The properties of the QPT have been investigated by using a mapping to a system with free fermions [26] and the real-space renormalization group analysis [27, 28]. Around the critical point, the Griffiths–McCoy (GM) singularity arises [29, 30] due to the presence of a statistically rare region where the spins are strongly coupled in the paramagnetic phase and decoupled in the ordered phase. The GM singularity leads to a continuously varying dynamical exponent in the disordered phase, which results in the divergence of susceptibility for a finite range of transverse-field strength. At the critical point, the characteristic time scale anomalously diverges, that is, the dynamical critical exponent is infinite. The extremely long time scale affects the performance of the QA. The QA performance of a disordered Ising chain has been measured by the density of kinks, where the up spin and the down spin are next to each other. The KZM implies that the kink density decays in power law with the logarithm of the annealing time [23–

*Electronic address: tatsuhiko.shirai@aoni.waseda.jp

†Electronic address: shu.tanaka@appi.keio.ac.jp

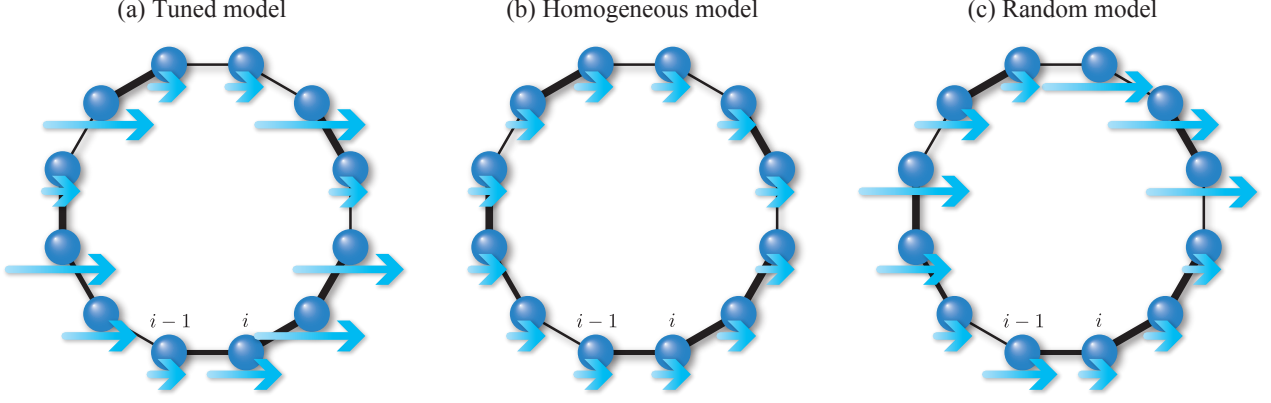


FIG. 1: (Color online) Schematics of the models considered in this paper: (a) tuned model given by Eq. (5), (b) homogeneous model given by Eq. (6), and (c) random model given by Eq. (7). The thickness of lines and the length of arrows represent the nearest-neighbor coupling strength $\{J_i\}_{i=1}^N$ and the transverse field strength $\{\Gamma_i\}_{i=1}^N$, respectively.

25]. The performance is worse compared to the case of the finite dynamical critical exponent, in which the kink density decays in power law with the annealing time.

In the present paper, we discuss properties of the QPT and the QA when the strengths of transverse fields are tuned depending on the spins. As presented in Fig. 1(a), we set the strength of the transverse field on each spin in proportion to the strength of the coupling connecting the spin. We find that the dynamical critical exponent is finite in this model in contrast to the previous studies [for comparison with our model, see Figs. 1(b) and (c)], and it depends on the distribution of the nearest-neighbor coupling strength. We verify the KZM through a numerical study of QA, which implies that the performance of the QA is improved by appropriately tuning the transverse field on each spin.

The present work is related to recent studies on QA using an inhomogeneous transverse field. Motivated by the implementation of an inhomogeneous transverse field on an experimental quantum annealer [31, 32], a wide variety of strategies to improve the performance of QA have been proposed [7, 33–39]. One strategy is to apply a stronger transverse field to spins strongly coupled to the rest of the system than those weakly coupled [39]. We give a formulation based on this strategy in a specific model, which will be helpful for studying the effect of inhomogeneous transverse field on more general and complicated models.

The paper is organized as follows. Sec. II introduces our model and two other models investigated in previous studies. Sec. III gives a finite-size scaling to estimate the critical exponents that characterize the diverging time scale and the diverging length scale at critical point. Sec. IV shows a result of QA in terms of kink density. Sec. V is dedicated to conclude our study with a future direction. Appendix A shows the details of a mapping from a spin system to a free fermion system. Appendix B gives a detail of the dynamical exponent around the critical point with analytical argument. Appendix C

shows the performance of QA in terms of residual energy.

II. MODELS

The purpose of our study is to investigate the effect of tuned inhomogeneous transverse field on properties of QPT and performance of QA through a prototypical model. Thus, we consider an Ising model on a one-dimensional chain of N spins under transverse fields. The Hamiltonian is given by

$$H = H_c + H_q, \quad (1)$$

$$H_c = - \sum_{i=1}^N J_i \sigma_{i-1}^z \sigma_i^z, \quad (2)$$

$$H_q = - \sum_{i=1}^N \Gamma_i \sigma_i^x, \quad (3)$$

where $\vec{\sigma}_i = (\sigma_i^x, \sigma_i^y, \sigma_i^z)$ is the Pauli matrix, and the periodic boundary condition is imposed, i.e. $\vec{\sigma}_0 = \vec{\sigma}_N$. The number of spins N is assumed to be even. The nearest-neighbor coupling strength and the transverse-field strength are denoted by $\{J_i\}_{i=1}^N$ and $\{\Gamma_i\}_{i=1}^N$, respectively. The coupling strength is chosen from a uniform distribution over $(J, 1]$, i.e.

$$\pi(J_i) = \begin{cases} (1-J)^{-1} & \text{for } J < J_i \leq 1, \\ 0 & \text{otherwise.} \end{cases} \quad (4)$$

We consider two different cases: $J = 0$ and $J > 0$. The former and the latter are referred to as strong disorder and weak disorder, respectively. Here, we adopt $J = 0.2$ in the numerical calculation for the case of weak disorder. In our model, which is referred to as tuned model [see Fig. 1(a)], we assume

$$\Gamma_i = \Gamma J_i \quad (\text{Tuned model}). \quad (5)$$

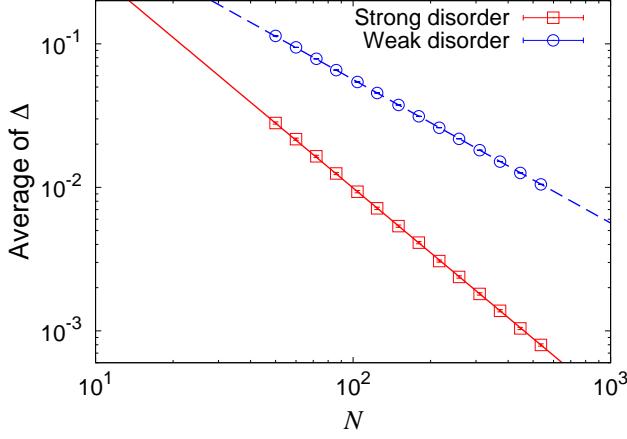


FIG. 2: (Color online) The system-size dependences of the average of energy gap $\overline{\Delta}$ at the critical point for (a) the model with strong disorder (red squares) and (b) the model with weak disorder (blue circles). The bold and dashed lines are the guides to show $\overline{\Delta} \sim N^{-3/2}$ and $\overline{\Delta} \sim N^{-1}$, respectively. Each data is obtained by averaging 1,000 realizations.

The transverse-field strength on a spin i is proportional to the coupling strength connecting spins $i-1$ and i , and its overall strength is controlled by Γ .

For the comparison of tuned model, we consider two other models: one uses a homogeneous strength of transverse field [see Fig. 1(b)],

$$\Gamma_i = \Gamma \quad (\text{Homogeneous model}), \quad (6)$$

and the other uses a random field where the strength is chosen according to the distribution of the coupling strength [see Fig. 1(c)], i.e.

$$\pi\left(\frac{\Gamma_i}{\Gamma}\right) = \pi(J_i) \quad (\text{Random model}). \quad (7)$$

It is noted that in the second model, the distributions of $\{\Gamma_i\}$ and $\{J_i\}$ are independent of each other. In the following, we refer to each model as homogeneous model [23, 27, 28] and random model [24–28], respectively.

The ground state of H in Eq. (1) is the paramagnetic phase when $\Gamma > \Gamma_c$ and the ordered phase when $\Gamma < \Gamma_c$. The transition point is determined by [27, 40]

$$\overline{\ln J} = \overline{\ln \Gamma}, \quad (8)$$

where $\overline{\ln J}$ and $\overline{\ln \Gamma}$ are the averages of $\ln J_i$ and $\ln \Gamma_i$ over the realization of disorder. Namely, $\Gamma_c = 1$ in tuned model and random model [24–28], and $\Gamma_c = e^{-1} J^{-J/(1-J)}$ in homogeneous model [23, 27, 28].

III. FINITE-SIZE SCALING

In this section, we investigate the properties of QPT in tuned model using the finite-size scaling. The diverging

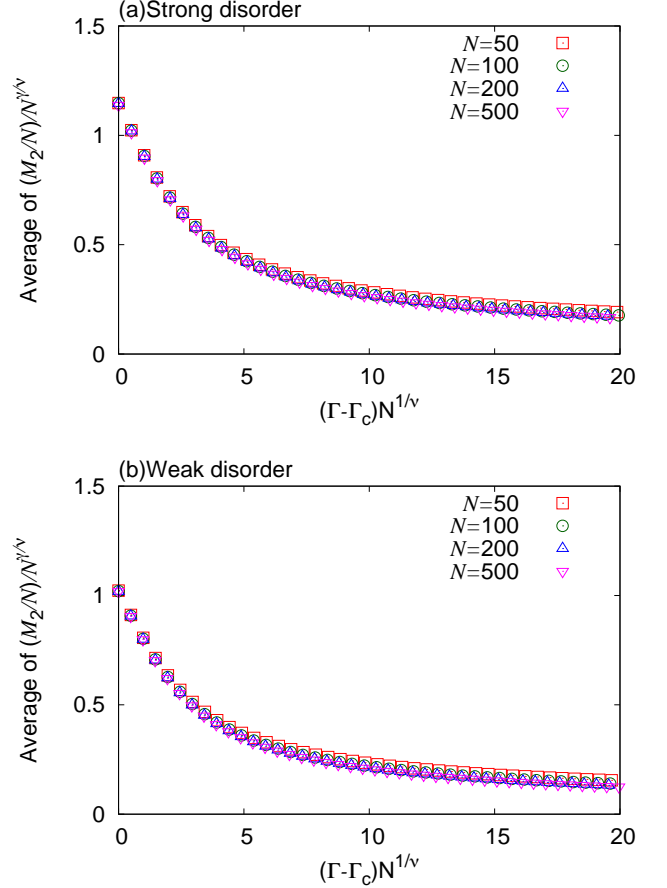


FIG. 3: (Color online) The scaling plots of the square of magnetization \overline{M}_2 in disordered phase for (a) the model with strong disorder and (b) the model with weak disorder. The critical exponents are set as (a) $\nu = 0.995$ and $\gamma = 0.690$ and (b) $\nu = 0.9957$ and $\gamma = 0.7495$, which are obtained by performing the finite-size scaling based on Bayesian inference [41, 42]. The data is averaged over 100 realizations of disorder.

time scale and the diverging length scale at the critical point are respectively described by the energy gap between the ground state and the first-excited state Δ and the correlation function C_{ij} ,

$$C_{ij} = \langle \sigma_i^z \sigma_j^z \rangle_g, \quad (9)$$

where $\langle O \rangle_g$ is the expectation value of an arbitrary operator O in the ground state (For the calculation details of Δ and C_{ij} , see Appendix A).

At the critical point, the average of Δ over the realization of disorder $\overline{\Delta}$ is described by

$$\overline{\Delta} \sim N^{-z}, \quad (10)$$

where z is the dynamical critical exponent. To consider the diverging length scale, instead of the correlation func-

tion, we use the square of magnetization,

$$M_2 = \sum_{i=1}^N \sum_{j=1}^N \langle \sigma_i^z \sigma_j^z \rangle_{\text{g}} = N + 2 \sum_{i < j}^N C_{ij}. \quad (11)$$

The square of magnetization corresponds to the susceptibility in the paramagnetic phase, i.e. $\Gamma \geq \Gamma_c$, and thus the average of M_2 over the random distribution $\overline{M_2}$ is assumed to scale as

$$\frac{\overline{M_2}}{N} = N^{\frac{\gamma}{\nu}} f((\Gamma - \Gamma_c) N^{\frac{1}{\nu}}), \quad (12)$$

where $f(\cdot)$ is a scaling function, and ν and γ are critical exponents of correlation length and susceptibility, respectively.

In the following, we provide a finite-size scaling of the energy gap $\overline{\Delta}$ and the square of magnetization $\overline{M_2}$ in the tuned model with strong disorder ($J = 0$) and weak disorder ($J = 0.2$).

We first consider the energy gap at the critical point. Figure 2 shows the N -dependences of $\overline{\Delta}$ for the system with strong disorder and weak disorder. The data are well described by the scaling,

$$\begin{cases} \overline{\Delta} \sim N^{-3/2} \text{ (strong disorder),} \\ \overline{\Delta} \sim N^{-1} \text{ (weak disorder),} \end{cases} \quad (13)$$

which implies that $z = 3/2$ for the case of strong disorder and $z = 1$ for the case of weak disorder, respectively. It is noted that the dynamical exponent $z = 1$ is the same as the one of the pure transverse-field Ising model. The origin of difference of z between the model with strong disorder and the model with weak disorder is discussed in Appendix B.

Next, we study the square of magnetization in the paramagnetic phase, i.e. $\Gamma \geq \Gamma_c$. We give scaling plots of $\overline{M_2}/N$ for the model with strong disorder [Fig. 3(a)] and the model with weak disorder [Fig. 3(b)]. We determine the critical exponents ν and γ by performing the finite-size scaling based on Bayesian inference [41, 42]. We obtain

$$\begin{cases} \nu = 0.995(2), & \gamma = 0.690(2) \text{ (strong disorder),} \\ \nu = 0.9957(5) & \gamma = 0.7495(4) \text{ (weak disorder),} \end{cases}$$

where the values of parenthesis denote the standard deviation. The values of ν in both models are close to the one of the pure transverse-field Ising model where $\nu = 1$. In the model with weak disorder, the value of γ is also close to the pure transverse-field Ising model where $\gamma = 3/4$ [43].

IV. QUANTUM ANNEALING

In this section, we show numerical results of performing the QA, and compare the performance of QA among

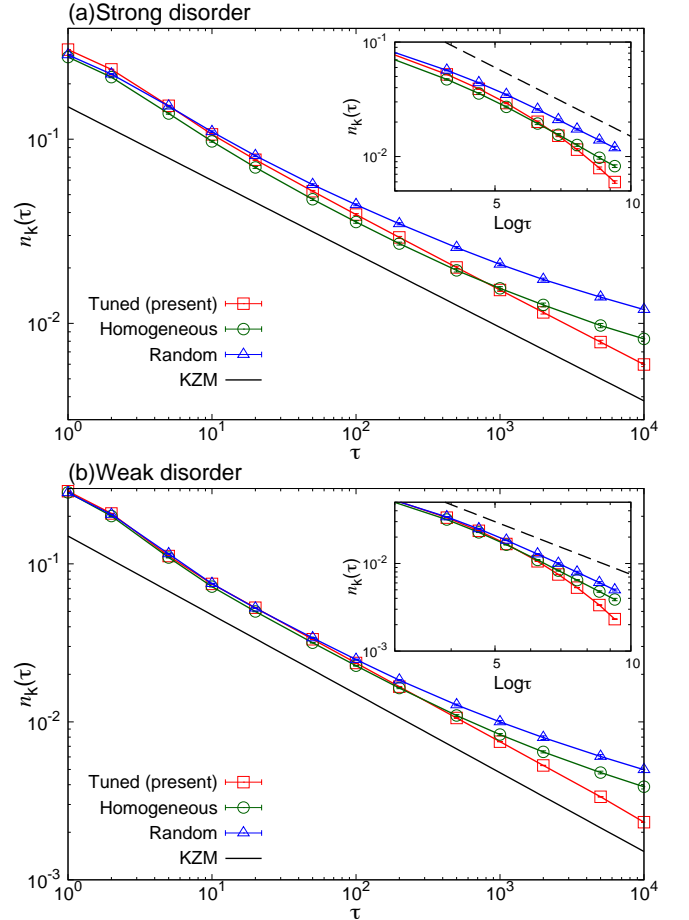


FIG. 4: (Color online) τ -dependences of kink density in three models: red squares [tuned model in Eq. (5)], green circles [homogeneous model in Eq. (6)], and blue triangles [random model in Eq. (7)]. (a) The model with strong disorder. The bold line shows the prediction of the KZM in Eq. (16) with $z = 3/2$ and $\nu = 0.995$. (inset) $n_k(\tau)$ vs $\log \tau$. The dashed line is a guide to show the dependence $n_k(\tau) \sim (\log \tau)^{-2}$. (b) The model with weak disorder. The bold line shows the prediction of the KZM in Eq. (16) with $z = 1$ and $\nu = 0.9957$. (inset) $n_k(\tau)$ vs $\log \tau$. The dashed line is a guide to show the dependence $n_k(\tau) \sim (\log \tau)^{-2}$. In each figure, the data is averaged over 20 realizations of disorder.

tuned model, homogeneous model, and random model. In the QA, the strength of transverse field is assumed to decrease with time from $\Gamma = \Gamma_0 (> \Gamma_c)$ to $\Gamma = 0$ as

$$\Gamma(t) = \Gamma_0 \left(1 - \frac{t}{\tau} \right), \quad (14)$$

where τ is the annealing time. In each model, we set $N = 500$ and the initial state to be the ground state of the Hamiltonian in Eq. (1) at $\Gamma_0 = 2\Gamma_c$. It is noted that Γ_c depends on the models (see the end of Sec. II).

The performance of QA is measured by the density of kink, where the up spin and the down spin are next to each other. The operator corresponding to the kink

density is defined by

$$\hat{n}_k = \frac{1}{2N} \sum_{i=1}^N (1 - \sigma_{i-1}^z \sigma_i^z), \quad (15)$$

and its expectation value after the annealing is denoted by $n_k(\tau)$ [For the calculation details of $n_k(\tau)$, see Appendix A].

The KZM relates $n_k(\tau)$ to the dynamical critical exponents as

$$n_k(\tau) \sim \tau^{-\frac{\nu}{1+z\nu}} \text{ (KZM)}. \quad (16)$$

Here, the large system size and the long annealing time are assumed. In the tuned model, the exponent in Eq. (16) is estimated by using the critical exponents z and ν obtained in Sec. III: The exponent is $-0.399(1)$ in the model with strong disorder and it is $-0.4989(2)$ in the model with weak disorder. In homogeneous model and random model, the dynamical exponent is infinite, and there additional analysis is necessary to obtain the correct asymptotic form of $n_k(\tau)$ [23, 24]. It is given by

$$n_k(\tau) \sim (\log \tau)^{-2} \text{ (KZM)}. \quad (17)$$

In Fig. 4(a), we show τ -dependences of kink density for the strong disorder case. In each model, the slope of the line increases with τ in the log-log plot. The slope corresponds to the exponent in Eq. (16). In the tuned model, the exponent approaches a constant value. We use the data for $\tau \geq 10^3$ and obtain

$$n_k(\tau) \sim \tau^{-0.41(1)} \text{ (Strong disorder)}, \quad (18)$$

which is consistent with the prediction of the KZM in Eq. (16). On the other hand, in homogeneous model and random model, the slope continuously increases in the time domain up to $\tau \leq 10^4$. In the inset of figure, we show the kink density as a function of $\log \tau$. We find the linear dependences in the log-log plot in homogeneous model and random model for large τ . We use the data for $\tau \geq 10^3$ and estimate the exponents as $-2.2(1)$ in homogeneous model and $-2.0(1)$ in random model, which are close to the prediction of KZM in Eq. (17).

In Fig. 4(b), we show τ -dependences of kink density for the weak disorder case. In the tuned model, the data shows the linear dependence in the log-log plot. We use the data for $\tau \geq 10^3$ and obtain

$$n_k(\tau) \sim \tau^{-0.5080(2)} \text{ (Weak disorder)}, \quad (19)$$

which well agrees with the prediction of the KZM in Eq. (16). As in the model with strong disorder, in homogeneous model and random model, the slope continuously increases with τ . In the inset of figure showing $\log \tau$ vs $n_k(\tau)$, we find the linear dependences in the log-log plot in these models for large τ . We use the data for $\tau \geq 10^3$ and estimate the exponents as $-2.7(2)$ in homogeneous model and $-2.4(1)$ in random model, which are slightly

smaller than that of KZM in Eq. (17). We expect that the reason for this discrepancy is due to finite-size effects.

In Appendix C, we present the QA performance of tuned model in terms of the residual energy. As is measured by the kink density, τ -dependence of the residual energy is qualitatively different between the model with strong disorder and the model weak disorder.

V. CONCLUSION AND OUTLOOK

We investigated the effect of tuned inhomogeneous transverse field in a disordered Ising chain on properties of the QPT and the QA. We found that properties of the QPT and the QA depend on the distribution of the nearest-neighbor coupling strength: the model with strong disorder and the model with weak disorder [see Eq. (4)]. We obtained the critical exponents z , ν , and γ from the finite-size scaling. In contrast to previous studies where the transverse field is homogeneous over spins or randomly distributed independently of the coupling strength, we found that the dynamical critical exponents z are finite: $z = 3/2$ in the model with strong disorder and $z = 1$ in the model with weak disorder. The difference of z is attributed to the presence of weak bond, i.e. $J_i \simeq 0$, in the model with strong disorder (see details in Appendix B). In the model with weak disorder, the critical exponents, z , ν , and γ , are almost the same as ones in the model without disorder, that is, the pure transverse-field Ising model. Using the estimated critical exponents z and ν , we verified the KZM through the numerical simulation of QA, and there demonstrated the importance of tuning the transverse field on each site to improve the performance of QA.

There remains an issue to be studied. It is important to study the effect of the tuned inhomogeneous transverse field on the model in d -dimension ($d \geq 2$) [44–47], where spin glass phase can appear due to the presence of frustration.

Acknowledgments

T. S. thanks Kensuke Tamura for fruitful discussion. T. S. was partially supported by JSPS KAKENHI Grant Number 18K13466. S. T. was partially supported by JSPS KAKENHI Grant Number 19H01553. This paper is partially based on the results obtained from a project commissioned by the New Energy and Industrial Technology Development Organization (NEDO). T. S. and S. T. thank the Supercomputer Center, the Institute for Solid State Physics, the University of Tokyo and the supercomputers at Yukawa Institute for Theoretical Physics, for the use of the facilities.

Note added.—While completing this work, we became aware of a paper by S. Knysh et al. [48] in which similar results were obtained using different approaches.

Appendix A: Calculation details: A mapping from a spin system to a free fermion system

We show the details to calculate the energy gap, the correlation function, and the dynamics of kink density in QA using a transformation of a spin system to a free fermion system.

In the Jordan–Wigner transformation [49], the fermion operator is described by

$$\begin{cases} c_j = -\frac{i}{2} \prod_{k=1}^{j-1} (-\sigma_k^x)(\sigma_j^y - i\sigma_j^z), \\ c_j^\dagger = \frac{i}{2} \prod_{k=1}^{j-1} (-\sigma_k^x)(\sigma_j^y + i\sigma_j^z), \end{cases} \quad (\text{A1})$$

where c_j and c_j^\dagger are the annihilation and the creation operator of the fermion at site j , respectively. The Hamiltonian in Eq. (1) is then written in the fermion operators as

$$\begin{aligned} H = & - \sum_{i=2}^N J_i (c_{i-1}^\dagger - c_{i-1})(c_i^\dagger + c_i) \\ & + (-1)^{N_f} J_1 (c_N^\dagger - c_N)(c_1^\dagger + c_1) \\ & - \sum_{i=1}^N \Gamma_i (2c_i^\dagger c_i - 1), \end{aligned} \quad (\text{A2})$$

where $N_f = \sum_{i=1}^N c_i^\dagger c_i$. Notice that although N_f is not conserved by the Hamiltonian, $(-1)^{N_f}$ is conserved: $(-1)^{N_f}$ is a constant of motion with value 1 or -1 . Throughout this study, we consider a subspace where $(-1)^{N_f} = 1$. The ground state of system with large Γ belongs to this subspace because each site is occupied by the fermion, and thus $(-1)^{N_f} = (-1)^N = 1$. Here, the assumption of even N is used. The Hamiltonian in this subspace is described in a quadratic form of fermion operators as

$$H = \sum_{i=1}^N \sum_{j=1}^N \left[c_i^\dagger A_{ij} c_j + \frac{B_{ij}}{2} (c_i^\dagger c_j^\dagger + c_j c_i) \right] + \text{const.}, \quad (\text{A3})$$

where

$$\begin{cases} A_{i,i} = -2\Gamma_i, \\ A_{i-1,i} = -J_i, A_{i,i-1} = -J_i, \text{ for } 2 \leq i \leq N, \\ A_{N,1} = J_1, A_{1,N} = J_1, \\ \text{otherwise } 0, \end{cases}$$

and

$$\begin{cases} B_{i-1,i} = -J_i, B_{i,i-1} = J_i \text{ for } 2 \leq i \leq N, \\ B_{N,1} = J_1, B_{1,N} = -J_1, \\ \text{otherwise } 0. \end{cases}$$

Here, $\{A_{ij}\}$ and $\{B_{ij}\}$ are regarded as the (i, j) -element of a matrix A and a matrix B , respectively. The matrix

A is a symmetric matrix and B is an alternative matrix. In the following, we denote the (i, j) -element of a matrix M by $[M]_{ij}$.

Since the Hamiltonian is written in the quadratic form, it is transformed into a diagonal form,

$$H = \sum_{k=1}^N \Lambda_k \eta_k^\dagger \eta_k + \text{const.}, \quad (\text{A4})$$

by using the Bogoliubov transformation,

$$\begin{aligned} \eta_k &= \sum_{i=1}^N (g_{ki} c_i + h_{ki} c_i^\dagger), \\ \eta_k^\dagger &= \sum_{i=1}^N (g_{ki} c_i^\dagger + h_{ki} c_i), \end{aligned} \quad (\text{A5})$$

where $g_{ki}, h_{ki} \in \mathbb{R}$. Here, η_k and η_k^\dagger satisfy the anticommutation relation of fermions, and $\Lambda_k (> 0)$ is regarded as a quasienergy of quasiparticle. The quasienergy Λ_k is arranged in ascending order, i.e., $0 \leq \Lambda_1 \leq \Lambda_2 \leq \dots$. The coefficients g_{ki} and h_{ki} satisfy

$$\begin{aligned} \Lambda_k g_{ki} &= \sum_{j=1}^N (A_{ij} g_{kj} + B_{ij} h_{kj}), \\ \Lambda_k h_{ki} &= - \sum_{j=1}^N (B_{ij} g_{kj} + A_{ij} h_{kj}). \end{aligned} \quad (\text{A6})$$

In terms of the new variables,

$$\phi_{ki} = g_{ki} + h_{ki}, \quad \psi_{ki} = g_{ki} - h_{ki}, \quad (\text{A7})$$

the coupled equations are

$$\begin{aligned} \sum_{j=1}^N [A + B]_{ij} \phi_{kj} &= \Lambda_k \psi_{ki}, \\ \sum_{j=1}^N [A - B]_{ij} \psi_{kj} &= \Lambda_k \phi_{ki}. \end{aligned} \quad (\text{A8})$$

The problem is reduced to an eigenvalue problem [49, 50]:

$$\sum_{j=1}^N [(A - B)(A + B)]_{ij} \phi_{kj} = \Lambda_k^2 \phi_{ki}. \quad (\text{A9})$$

For $\Lambda_k \neq 0$, Eq. (A9) is solved for $\{\phi_{ki}\}_{i=1}^N$, and $\{\psi_{ki}\}_{i=1}^N$ are obtained from

$$\psi_{ki} = \frac{1}{\Lambda_k} \sum_{j=1}^N [A + B]_{ij} \phi_{kj}. \quad (\text{A10})$$

For $\Lambda_k = 0$, $\{\phi_{ki}\}_{i=1}^N$ and $\{\psi_{ki}\}_{i=1}^N$ are determined by Eqs. (A8), their relative sign being arbitrary.

In the following, we give a brief review to obtain the energy gap Δ and the correlation function C_{ij} in the language of fermions. The energy gap is obtained by

$$\Delta = \Lambda_1 + \Lambda_2, \quad (\text{A11})$$

since it is necessary to create two quasiparticles to keep the state being in the subspace where $(-1)^{N_f} = 1$. The correlation function C_{ij} for $j > i$ is given by [26, 49]

$$C_{ij} = \det G_{ij} \quad (\text{A12})$$

where G_{ij} is a matrix with $j-i$ dimension and its matrix element is given by

$$[G_{ij}]_{kl} = \langle (c_{i+k-1}^\dagger - c_{i+k-1})(c_{i+l}^\dagger + c_{i+l}) \rangle_g. \quad (\text{A13})$$

The labels k and l run from 1 to $j-i$.

Finally, the quantum dynamics in terms of the fermion operators is explained. The Hamiltonian is time dependent in QA, and thus we set

$$A_{ij} \rightarrow A_{ij}(t) \text{ and } B_{ij} \rightarrow B_{ij}(t). \quad (\text{A14})$$

The quantum dynamics is governed by the Heisenberg equation,

$$i \frac{d}{dt} c_{i,H}(t) = \sum_{j=1}^N (A_{ij}(t) c_{j,H}(t) + B_{ij}(t) c_{j,H}^\dagger(t)), \quad (\text{A15})$$

where $c_{i,H}(t)$ and $c_{i,H}^\dagger(t)$ denote the Heisenberg representation of the fermion operators c_i and c_i^\dagger . Then, we expand $c_{i,H}(t)$ by $\{c_j\}_{j=1}^N$ and $\{c_j^\dagger\}_{j=1}^N$ as

$$c_{i,H}(t) = \sum_{j=1}^N (u_{ij}(t) c_j + v_{ij}^*(t) c_j^\dagger), \quad (\text{A16})$$

where $u_{ij}(t), v_{ij}(t) \in \mathbb{C}$. Substituting it into the Heisenberg equation in Eq. (A15), the coefficients $u_{ij}(t)$ and $v_{ij}(t)$ obey linear differential equations [24, 51, 52],

$$\begin{aligned} \frac{d}{dt} u_{ij}(t) &= -i \sum_{k=1}^N (A_{ik}(t) u_{kj}(t) + B_{ik}(t) v_{kj}(t)), \\ \frac{d}{dt} v_{ij}(t) &= i \sum_{k=1}^N (A_{ik}(t) v_{kj}(t) + B_{ik}(t) u_{kj}(t)). \end{aligned} \quad (\text{A17})$$

This is the time-dependent generalization of the Bogoliubov-de Gennes equation. In the numerical simulation of QA, we have assumed the initial state to be the ground state of the initial Hamiltonian. It is then convenient to set the initial conditions of $u_{ij}(t)$ and $v_{ij}(t)$ as

$$u_{ij}(0) = g_{ij} \text{ and } v_{ij}(0) = h_{ij}, \quad (\text{A18})$$

where g_{ij} and h_{ij} are obtained by Eqs. (A4) and (A5) for the initial Hamiltonian.

The operator for the kink density [see Eq. (15)] is described by the fermion operators as

$$\begin{aligned} \hat{n}_k &= \frac{1}{2} - \frac{1}{2N} \sum_{i=2}^N (c_{i-1} - c_{i-1}^\dagger)(c_i + c_i^\dagger) \\ &\quad + \frac{1}{2N} (c_N - c_N^\dagger)(c_1 + c_1^\dagger). \end{aligned} \quad (\text{A19})$$

The expectation value of the kink density after QA with annealing time τ , $n_k(\tau)$, is given by

$$\begin{aligned} n_k(\tau) &= \frac{1}{2} - \frac{1}{2N} \sum_{i=2}^N \langle \psi_i | (c_{i-1,H}(\tau) - c_{i-1,H}^\dagger(\tau)) \\ &\quad \times (c_{i,H}(\tau) + c_{i,H}^\dagger(\tau)) | \psi_i \rangle \\ &\quad + \frac{1}{2N} \langle \psi_i | (c_{N,H}(\tau) - c_{N,H}^\dagger(\tau)) \\ &\quad \times (c_{1,H}(\tau) + c_{1,H}^\dagger(\tau)) | \psi_i \rangle \\ &= \frac{1}{2} - \frac{1}{2N} \sum_{j=1}^N \left[\sum_{i=2}^N (v_{i-1,j}(\tau) - u_{i-1,j}(\tau)) \right. \\ &\quad \times (u_{i,j}^*(\tau) + v_{i,j}^*(\tau)) \\ &\quad \left. + (v_{N,j}(\tau) - u_{N,j}(\tau))(u_{1,j}^*(\tau) + v_{1,j}^*(\tau)) \right], \end{aligned} \quad (\text{A20})$$

where $|\psi_i\rangle$ is the wave function of the initial state.

Appendix B: Dynamical exponents around the critical point

In this appendix, we discuss dynamical exponents of tuned model at Γ , $z(\Gamma)$, including the region apart from the critical point, i.e. $\Gamma \neq \Gamma_c$. We give a mathematical argument that determines an upper bound and a lower bound of dynamical exponents. We show that the bounds are different between the model with strong disorder and the model with weak disorder and the difference arises due to the presence of the weak bond, i.e. $J_i \simeq 0$, in the model with strong disorder.

We analyze the eigenvalues of the matrix $(A-B)(A+B)$ denoted by $\{\Lambda_k^2\}$ in Eq. (A9), which are related to the energy gap by $\Delta = \Lambda_1 + \Lambda_2$ in Eq. (A11). The matrix is explicitly given by

$$(A-B)(A+B) = 4\Gamma J T J, \quad (\text{B1})$$

where $J = \text{diag}(J_1, \dots, J_N)$ and

$$[T]_{ij} = \begin{cases} \Gamma + \Gamma^{-1} & \text{for } i = j, \\ 1 & \text{for } |i - j| = 1, \\ -1 & \text{for } (i, j) = (1, N) \text{ and } (N, 1), \\ \text{otherwise } 0. & \end{cases} \quad (\text{B2})$$

We first discuss the energy gap in the limits of $\Gamma \rightarrow 0$ and $\Gamma \rightarrow \infty$. In the limit of $\Gamma \rightarrow 0$,

$$\lim_{\Gamma \rightarrow 0} 4\Gamma J T J = 4J^2. \quad (\text{B3})$$

The energy gap is given by

$$\lim_{\Gamma \rightarrow 0} \Delta = 2(J^{(1)} + J^{(2)}), \quad (\text{B4})$$

where $J^{(1)}$ and $J^{(2)}$ are the lowest and the second lowest values in the set of $\{J_i\}$. On the other hand, in the limit of $\Gamma \rightarrow \infty$,

$$\lim_{\Gamma \rightarrow \infty} 4\Gamma^{-1} J T J = 4J^2, \quad (\text{B5})$$

and the energy gap is given by

$$\lim_{\Gamma \rightarrow \infty} \Gamma^{-1} \Delta = 2(J^{(1)} + J^{(2)}). \quad (\text{B6})$$

The energy gaps in these limits are also obtained by looking at Eq. (1).

We next discuss a lower bound of the energy gap for nonzero Γ . Here, we introduce a set of vectors $V = \{\vec{x}_1, \dots, \vec{x}_N\}$, where the j -th element of \vec{x}_n denoted by x_{nj} is given by

$$x_{nj} = C J_j^{-1} \exp\left(i \frac{\pi}{N} (2n-1)j\right) \text{ for } j = 1, \dots, N. \quad (\text{B7})$$

The normalization constant C is set as

$$C = \left(\sum_{i=1}^N J_i^{-2} \right)^{-\frac{1}{2}} \quad (\text{B8})$$

so that $(\vec{x}_n, \vec{x}_n) = 1$, where $(\vec{a}, \vec{b}) := \sum_{j=1}^N a_j^* b_j$ is an inner product. The vectors satisfy the following relation,

$$(\vec{x}_n, J T J \vec{x}_m) = N C^2 \left(\Gamma + \Gamma^{-1} + 2 \cos \frac{\pi(2n-1)}{N} \right) \delta_{n,m}, \quad (\text{B9})$$

where $\delta_{n,m}$ is the Kronecker delta. The set V is a basis since the determinant of a matrix X with a matrix element $[X]_{ij} = x_{ij}$ is nonzero, i.e.

$$\det X = C^N \left(\prod_{i=1}^N J_i^{-1} \right) N^{\frac{N}{2}} > 0. \quad (\text{B10})$$

Then, any vector \vec{y} with $\|\vec{y}\| = 1$ can be expressed by $\{\vec{x}_n\}$ as

$$\vec{y} = \frac{\sum_{n=1}^N \alpha_n \vec{x}_n}{\left\| \sum_{n=1}^N \alpha_n \vec{x}_n \right\|}, \quad (\text{B11})$$

where $\alpha_n \in \mathbb{C}$ and $\|\vec{a}\| = \sqrt{(\vec{a}, \vec{a})}$, respectively. The expectation value of $J T J$ with respect to \vec{y} is bounded

by

$$\begin{aligned} (\vec{y}, J T J \vec{y}) &= \frac{\sum_{n=1}^N N |\alpha_n|^2 C^2 \left(\Gamma + \Gamma^{-1} + 2 \cos \frac{(2n-1)\pi}{N} \right)}{\left\| \sum_{n=1}^N \alpha_n \vec{x}_n \right\|^2}, \\ &\geq N \left(\Gamma + \Gamma^{-1} - 2 \cos \frac{\pi}{N} \right) C^2 \frac{\sum_{n=1}^N |\alpha_n|^2}{\left\| \sum_{n=1}^N \alpha_n \vec{x}_n \right\|^2}, \\ &\geq \left(\Gamma + \Gamma^{-1} - 2 \cos \frac{\pi}{N} \right) C^2. \end{aligned} \quad (\text{B12})$$

From the second line to the third line, we have used the Cauchy-Schwarz inequality,

$$\left\| \sum_{n=1}^N \alpha_n \vec{x}_n \right\|^2 \quad (\text{B13})$$

$$\begin{aligned} &\leq \sum_{m=1}^N \sum_{n=1}^N |\alpha_m| |\alpha_n| |(\vec{x}_m, \vec{x}_n)|, \\ &\leq \sqrt{\sum_{m=1}^N \sum_{n=1}^N |\alpha_m|^2 |\alpha_n|^2} \sqrt{\sum_{m=1}^N \sum_{n=1}^N |(\vec{x}_m, \vec{x}_n)|^2}, \\ &\leq N \sum_{n=1}^N |\alpha_n|^2. \end{aligned} \quad (\text{B14})$$

Eq. (B12) gives a lower bound of the energy gap as

$$\Delta \geq 2C \sqrt{4\Gamma \left(\Gamma + \Gamma^{-1} - 2 \cos \frac{\pi}{N} \right)}. \quad (\text{B15})$$

Then, we discuss an upper bound of the energy gap for nonzero Γ . To give an upper bound of Δ , we use a variational principle that for $\vec{\psi}_1$ and $\vec{\psi}_2$ satisfying $\|\vec{\psi}_1\| = 1$, $\|\vec{\psi}_2\| = 1$, and $(\vec{\psi}_1, \vec{\psi}_2) = 0$,

$$4\Gamma[(\vec{\psi}_1, J T J \vec{\psi}_1) + (\vec{\psi}_2, J T J \vec{\psi}_2)] \geq \Lambda_1^2 + \Lambda_2^2. \quad (\text{B16})$$

In the following, we derive the variational principle [55]. We denote $\vec{\phi}_k$ by the eigenvector of $4\Gamma J T J$ corresponding to the eigenvalue Λ_k^2 and assume the orthonormality, i.e., $(\vec{\phi}_k, \vec{\phi}_\ell) = \delta_{k,\ell}$. Then, we expand $\vec{\psi}_1$ and $\vec{\psi}_2$ in the eigenbasis as

$$\vec{\psi}_i = \sum_{k=1}^N \alpha_{i,k} \vec{\phi}_k =: \alpha_{i,1} \vec{\phi}_1 + \alpha_{i,2} \vec{\phi}_2 + \vec{\xi}_i, \quad (\text{B17})$$

where $\alpha_{i,k} \in \mathbb{C}$. Due to the orthonormality of $\{\vec{\phi}_k\}$ and $\|\vec{\psi}_i\| = 1$, the coefficients satisfy

$$\sum_{k=1}^N |\alpha_{i,k}|^2 = 1. \quad (\text{B18})$$

Since $\vec{\psi}_1$ and $\vec{\psi}_2$ are orthogonal with each other,

$$\begin{aligned}
|\alpha_{1,\ell}||\alpha_{2,\ell}| &= \left| \sum_{\substack{k=1 \\ (k \neq \ell)}}^N \alpha_{1,k} \alpha_{2,k} \right| \\
&\leq \sum_{\substack{k=1 \\ (k \neq \ell)}}^N |\alpha_{1,k}| |\alpha_{2,k}| \\
&\leq \sqrt{\sum_{\substack{k=1 \\ (k \neq \ell)}}^N |\alpha_{1,k}|^2} \sqrt{\sum_{\substack{k=1 \\ (k \neq \ell)}}^N |\alpha_{2,k}|^2} \\
&= \sqrt{(1 - |\alpha_{1,\ell}|^2)(1 - |\alpha_{2,\ell}|^2)} \\
&\leftrightarrow 0 \leq 1 - (|\alpha_{1,\ell}|^2 + |\alpha_{2,\ell}|^2). \quad (\text{B19})
\end{aligned}$$

From the third line to the fourth line, we have used Eq. (B18). Since $(\vec{\phi}_1, \vec{\xi}_i) = (\vec{\phi}_2, \vec{\xi}_i) = 0$ by definition in Eq. (B17), we obtain

$$\begin{aligned}
\sum_{i=1}^2 (\vec{\xi}_i, 4\Gamma J T J \vec{\xi}_i) &\geq \Lambda_3^2 \sum_{i=1}^2 (\vec{\xi}_i, \vec{\xi}_i) \\
&= \Lambda_3^2 \sum_{i=1}^2 [1 - (|\alpha_{1,i}|^2 + |\alpha_{2,i}|^2)]. \quad (\text{B20})
\end{aligned}$$

Then, the left-hand side of Eq. (B16) is bounded by

$$\begin{aligned}
&4\Gamma[(\vec{\psi}_1, J T J \vec{\psi}_1) + (\vec{\psi}_2, J T J \vec{\psi}_2)] \\
&= \sum_{i=1}^2 (|\alpha_{1,i}|^2 + |\alpha_{2,i}|^2) \Lambda_i^2 + (\vec{\xi}_i, 4\Gamma J T J \vec{\xi}_i) \\
&\geq \sum_{i=1}^2 \Lambda_i^2 + [1 - (|\alpha_{1,i}|^2 + |\alpha_{2,i}|^2)] (\Lambda_3^2 - \Lambda_i^2) \\
&\geq \Lambda_1^2 + \Lambda_2^2. \quad (\text{B21})
\end{aligned}$$

We have used Eq. (B20) from the second line to the third line and Eq. (B19) from the third line to the fourth line.

We set $\vec{\psi}_1$ and $\vec{\psi}_2$ in Eq. (B16) as

$$\begin{cases} \vec{\psi}_1 = \vec{x}_{N/2}, \\ \vec{\psi}_2 = \frac{\vec{x}_{(N/2)+1} - (\vec{x}_{N/2}, \vec{x}_{(N/2)+1}) \vec{x}_{N/2}}{\sqrt{1 - |(\vec{x}_{N/2}, \vec{x}_{(N/2)+1})|^2}}, \end{cases}$$

which satisfy the condition of the variational principle. By substituting them into Eq. (B16), we obtain

$$\frac{4\Gamma N C^2 (\Gamma + \Gamma^{-1} - 2 \cos \frac{\pi}{N})}{1 - |(\vec{x}_{N/2}, \vec{x}_{(N/2)+1})|^2} \geq \Lambda_1^2 + \Lambda_2^2 \geq \Lambda_2^2. \quad (\text{B22})$$

Then, an upper bound of the energy gap is given by

$$\Delta \leq 2\Lambda_2 \leq 2C' \sqrt{4\Gamma N (\Gamma + \Gamma^{-1} - 2 \cos \frac{\pi}{N})}, \quad (\text{B23})$$

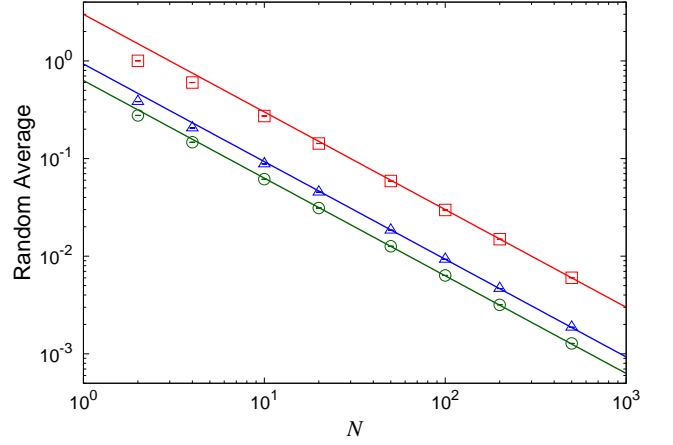


FIG. 5: (Color online) The system-size dependences of $\overline{J^{(1)} + J^{(2)}}$ (red squares), \overline{C} (green circles), and $\overline{C'}$ (blue triangle) for the model with strong disorder. The lines are the guide to show that the random averages are inversely proportional to the system size for large N . The average is taken from 10,000 realizations of disorder.

where

$$C' = \frac{C}{\sqrt{1 - |(\vec{x}_{N/2}, \vec{x}_{(N/2)+1})|^2}}. \quad (\text{B24})$$

To give an asymptotic form of energy gap for large N , we replace the random variables $J^{(1)} + J^{(2)}$, C , and C' by averages over the realization of disorder and study their large system-size asymptotic forms. The average of a random variable a is denoted by \bar{a} in the following. In Fig. 5, we plot the system-size dependences of the averages for the model with strong disorder. We perform a numerical integration using a Monte-Carlo sampling to take an average of the random variables [53]. For large N , we find

$$\overline{J^{(1)} + J^{(2)}} \sim N^{-1}, \quad \overline{C} \sim N^{-1}, \quad \text{and} \quad \overline{C'} \sim N^{-1}. \quad (\text{B25})$$

On the other hand, for the model with weak disorder, since the lowest value of J_i is finite, i.e. $J^{(1)} > J > 0$,

$$\overline{J^{(1)} + J^{(2)}} \sim N^0, \quad \overline{C} \sim N^{-\frac{1}{2}}, \quad \text{and} \quad \overline{C'} \sim N^{-\frac{1}{2}}. \quad (\text{B26})$$

The exponents for all the random variables are smaller in the model with strong disorder than the model with weak disorder due to the presence of the weak bond, that is, $J_i \simeq 0$.

From the above arguments, we discuss the dynamical exponents. The lower bound and the upper bound of the energy gap in Eqs. (B15) and (B23) determine an upper bound and a lower bound of the dynamical exponent. At the critical point, i.e. $\Gamma = \Gamma_c = 1$,

$$\Gamma + \Gamma^{-1} - 2 \cos \frac{\pi}{N} \sim N^{-2}, \quad (\text{B27})$$

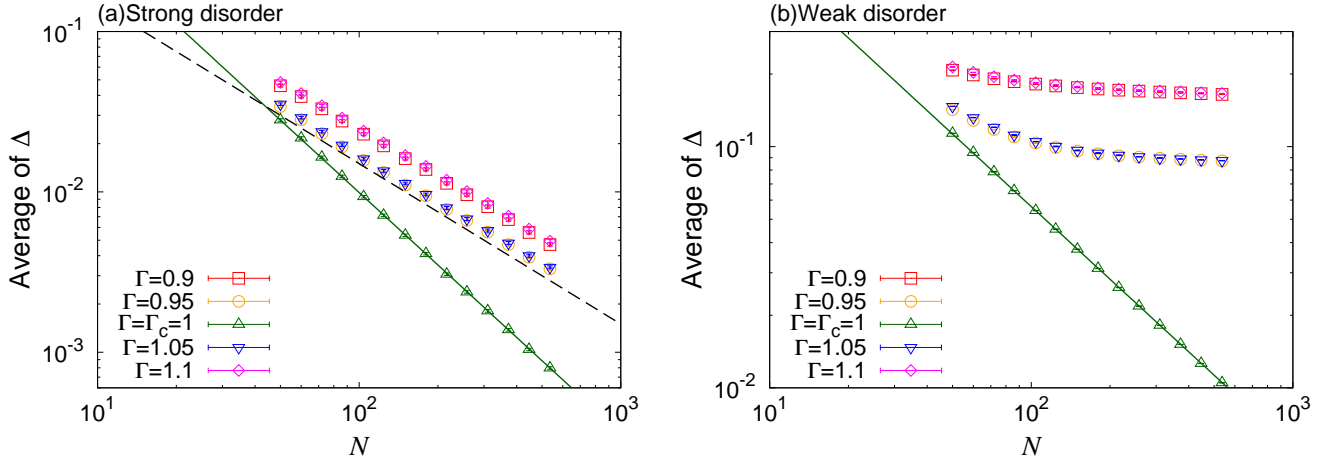


FIG. 6: (Color online) The system-size dependences of $\bar{\Delta}$ around the critical point. (a) The model with strong disorder is depicted. The solid line and the dashed line are guides to show $\bar{\Delta} \sim N^{-3/2}$ and $\bar{\Delta} \sim N^{-1}$, respectively. (b) The model with weak disorder is depicted ($J = 0.2$). The bold line is a guide to show $\bar{\Delta} \sim N^{-1}$. In each figure, the data is averaged over 1,000 realizations of disorder.

and then

$$\begin{cases} N^{-2} \lesssim \bar{\Delta} \lesssim N^{-\frac{3}{2}} \leftrightarrow \frac{3}{2} \leq z(\Gamma_c) \leq 2 & (\text{strong disorder}), \\ N^{-\frac{3}{2}} \lesssim \bar{\Delta} \lesssim N^{-1} \leftrightarrow 1 \leq z(\Gamma_c) \leq \frac{3}{2} & (\text{weak disorder}). \end{cases}$$

The dynamical exponents obtained in numerical results agree with the lower bounds in both models with strong disorder and weak disorder. Apart from the critical point, i.e. $\Gamma \neq \Gamma_c$, since the value in Eq. (B27) is the order of N^0 ,

$$\begin{cases} N^{-1} \lesssim \bar{\Delta} \lesssim N^{-\frac{1}{2}} \leftrightarrow \frac{1}{2} \leq z(\Gamma \neq \Gamma_c) \leq 1 & (\text{strong disorder}), \\ N^{-\frac{1}{2}} \lesssim \bar{\Delta} \lesssim N^0 \leftrightarrow 0 \leq z(\Gamma \neq \Gamma_c) \leq \frac{1}{2} & (\text{weak disorder}). \end{cases}$$

In the limit of $\Gamma \rightarrow 0$ and $\Gamma \rightarrow \infty$, the dynamical exponents [see Eqs. (B4), (B6), (B25), and (B26)] are

$$\begin{cases} \bar{\Delta} \sim N^{-1} \leftrightarrow \lim_{\Gamma \rightarrow 0} z(\Gamma) = \lim_{\Gamma \rightarrow \infty} z(\Gamma) = 1 & (\text{strong disorder}), \\ \bar{\Delta} \sim N^{-0} \leftrightarrow \lim_{\Gamma \rightarrow 0} z(\Gamma) = \lim_{\Gamma \rightarrow \infty} z(\Gamma) = 0 & (\text{weak disorder}). \end{cases}$$

Thus, the dynamical exponents in the limits agree with the upper bound in the model with strong disorder and the lower bound in the model with weak disorder. In Fig. 6, we give N -dependences of $\bar{\Delta}$ that show dynamical exponents around the critical point for the model with strong disorder [Fig. 6(a)] and the model with weak disorder [Fig. 6(b)]. The figure implies that the dynamical exponents apart from the critical point are constant and the

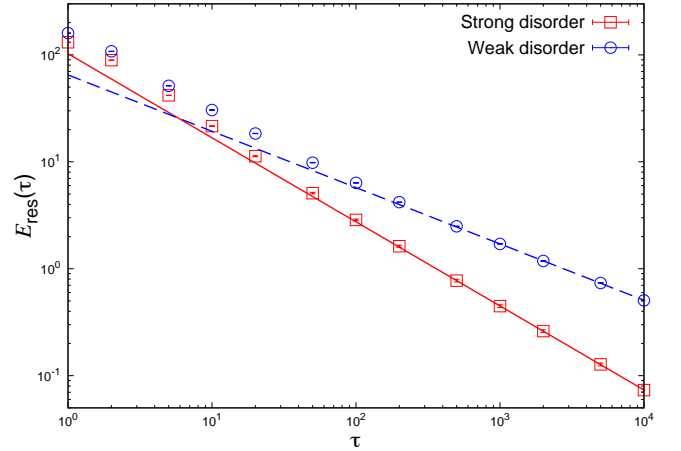


FIG. 7: (Color online) The dependences of residual energy $E_{\text{res}}(\tau)$ on the annealing time τ for the model with (a) strong disorder (red squares) and (b) weak disorder (blue circles). The solid line shows $E_{\text{res}}(\tau) \sim \tau^{-0.79}$ and the dashed line shows $E_{\text{res}}(\tau) \sim \tau^{-0.527}$, respectively. Each data is averaged over 20 realizations of disorder.

same as those of limiting cases, i.e. $z(\Gamma \neq \Gamma_c) = 1$ for the model with strong disorder and gapped [$z(\Gamma \neq \Gamma_c) = 0$] for the model with weak disorder.

Appendix C: Residual energy

In this appendix, we show τ -dependence of residual energy in tuned model with strong disorder and weak disorder. The residual energy measures the performance of QA as well as the kink density given by Eq. (15). It is

defined by

$$E_{\text{res}}(\tau) = \langle \psi(\tau) | \sum_{i=1}^N J_i \sigma_{i-1}^z \sigma_i^z | \psi(\tau) \rangle - E_g, \quad (\text{C1})$$

where $|\psi(\tau)\rangle$ is the wave function of system after QA with annealing time τ and E_g is the ground-state energy of the random Ising chain, i.e.

$$E_g = - \sum_{i=1}^N J_i. \quad (\text{C2})$$

By using a mapping from a spin operator to a fermion operator (see Appendix A), the residual energy is written as

$$\begin{aligned} E_{\text{res}}(\tau) = \sum_{j=1}^N \left[\sum_{i=2}^N -J_i (v_{i-1,j}(\tau) - u_{i-1,j}(\tau)) \right. \\ \times (u_{i,j}^*(\tau) + v_{i,j}^*(\tau)) \\ \left. + J_1 (v_{N,j}(\tau) - u_{N,j}(\tau)) \right. \\ \left. \times (u_{1,j}^*(\tau) + v_{1,j}^*(\tau)) \right] - E_g. \end{aligned} \quad (\text{C3})$$

In Fig. 7, we plot the dependences of the residual energy $E_{\text{res}}(\tau)$ on annealing time τ for the model with strong disorder and the model with weak disorder. In a log-log plot, we find the linear dependences in both models for large τ . We use the data for $\tau \geq 10^3$ and obtain

$$\begin{cases} E_{\text{res}}(\tau) \sim \tau^{-0.79(2)} \text{ (strong disorder),} \\ E_{\text{res}}(\tau) \sim \tau^{-0.527(3)} \text{ (weak disorder).} \end{cases} \quad (\text{C4})$$

In the model with strong disorder, the exponent for residual energy is about twice the exponent for kink density, which indicates that the kink is created more easily for the bond with small coupling strength J_i . On the other hand, in the model with weak disorder, the exponent for residual energy is almost the same as that for kink density, which is also observed in the pure transverse-field Ising model.

-
- [1] T. Kadowaki and H. Nishimori, Phys. Rev. E **58**, 5355 (1998).
 - [2] S. Tanaka, R. Tamura, and B. K. Chakrabarti, Quantum spin glasses, annealing and computation (Cambridge University Press, 2017).
 - [3] A. Messiah, Quantum mechanics: volume II (North-Holland Publishing Company Amsterdam, 1962).
 - [4] S. Sachdev, Quantum phase transitions (Wiley Online Library, 2007).
 - [5] T. Jörg, F. Krzakala, J. Kurchan, A. C. Maggs, and J. Pujos, EPL (Europhysics Letters) **89**, 40004 (2010).
 - [6] Y. Seki and H. Nishimori, Phys. Rev. E **85**, 051112 (2012).
 - [7] Y. Susa, Y. Yamashiro, M. Yamamoto, and H. Nishimori, Journal of the Physical Society of Japan **87**, 023002 (2018).
 - [8] Y. Yamashiro, M. Ohkuwa, H. Nishimori, and D. A. Lidar, Phys. Rev. A **100**, 052321 (2019).
 - [9] Y. Seki, S. Tanaka, and S. Kawabata, Journal of the Physical Society of Japan **88**, 054006 (2019).
 - [10] S. Watabe, Y. Seki, and S. Kawabata, Scientific Reports **10**, 146 (2020).
 - [11] T. W. B. Kibble, Journal of Physics A: Mathematical and General **9**, 1387 (1976).
 - [12] W. H. Zurek, Nature **317**, 505 (1985).
 - [13] W. H. Zurek, U. Dorner, and P. Zoller, Phys. Rev. Lett. **95**, 105701 (2005).
 - [14] J. Dziarmaga, Phys. Rev. Lett. **95**, 245701 (2005).
 - [15] A. Polkovnikov, Phys. Rev. B **72**, 161201 (2005).
 - [16] J. Dziarmaga, Advances in Physics **59**, 1063 (2010).
 - [17] A. Polkovnikov, K. Sengupta, A. Silva, and M. Vengalattore, Rev. Mod. Phys. **83**, 863 (2011).
 - [18] D. Chen, M. White, C. Borries, and B. DeMarco, Phys. Rev. Lett. **106**, 235304 (2011).
 - [19] S. Braun, M. Friesdorf, S. S. Hodgman, M. Schreiber, J. P. Ronzheimer, A. Riera, M. del Rey, I. Bloch, J. Eisert, and U. Schneider, Proceedings of the National Academy of Sciences **112**, 3641 (2015).
 - [20] M. Anquez, B. A. Robbins, H. M. Bharath, M. Boguslawski, T. M. Hoang, and M. S. Chapman, Phys. Rev. Lett. **116**, 155301 (2016).
 - [21] Y. Bando, Y. Susa, H. Oshiyama, N. Shibata, M. Ohzeki, F. J. Gómez-Ruiz, D. A. Lidar, A. del Campo, S. Suzuki, and H. Nishimori, arXiv:2001.11637 (2020).
 - [22] A. del Campo and W. H. Zurek, International Journal of Modern Physics A **29**, 1430018 (2014).
 - [23] J. Dziarmaga, Phys. Rev. B **74**, 064416 (2006).
 - [24] T. Caneva, R. Fazio, and G. E. Santoro, Phys. Rev. B **76**, 144427 (2007).
 - [25] S. Suzuki, Journal of Physics: Conference Series **302**, 012046 (2011).
 - [26] A. P. Young and H. Rieger, Phys. Rev. B **53**, 8486 (1996).
 - [27] D. S. Fisher, Phys. Rev. B **51**, 6411 (1995).
 - [28] D. S. Fisher, Phys. Rev. Lett. **69**, 534 (1992).
 - [29] R. B. Griffiths, Phys. Rev. Lett. **23**, 17 (1969).
 - [30] B. M. McCoy, Phys. Rev. Lett. **23**, 383 (1969).
 - [31] M. W. Johnson, M. H. S. Amin, S. Gildert, T. Lanting, F. Hamze, N. Dickson, R. Harris, A. J. Berkley, J. Johansson, P. Bunyk, et al., Nature **473**, 194 (2011).
 - [32] E. Andriyash, Z. Bian, F. A. Chudak, A. D. King, and W. G. Macready, in D-Wave Technical Report Series (2016), 14-1002A-B.
 - [33] J. Dziarmaga and M. M. Rams, New Journal of Physics **12**, 055007 (2010).

- [34] N. G. Dickson and M. H. Amin, Phys. Rev. A **85**, 032303 (2012).
- [35] A. del Campo, T. W. B. Kibble, and W. H. Zurek, Journal of Physics: Condensed Matter **25**, 404210 (2013).
- [36] M. M. Rams, M. Mohseni, and A. del Campo, New Journal of Physics **18**, 123034 (2016).
- [37] T. Lanting, A. D. King, B. Evert, and E. Hoskinson, Phys. Rev. A **96**, 042322 (2017).
- [38] F. J. Gómez-Ruiz and A. del Campo, Phys. Rev. Lett. **122**, 080604 (2019).
- [39] J. I. Adame and P. L. McMahon, Quantum Science and Technology **5**, 035011 (2020).
- [40] R. Shankar and G. Murthy, Phys. Rev. B **36**, 536 (1987).
- [41] K. Harada, Phys. Rev. E **84**, 056704 (2011).
- [42] K. Harada, Phys. Rev. E **92**, 012106 (2015).
- [43] P. Pfeuty, Annals of Physics **57**, 79 (1970).
- [44] H. Rieger and A. P. Young, Phys. Rev. B **54**, 3328 (1996).
- [45] M. Guo, R. N. Bhatt, and D. A. Huse, Phys. Rev. B **54**, 3336 (1996).
- [46] C. Pich, A. P. Young, H. Rieger, and N. Kawashima, Phys. Rev. Lett. **81**, 5916 (1998).
- [47] K. Nishimura, H. Nishimori, and H. G. Katzgraber, arXiv:2006.16219 (2020).
- [48] S. Knysh, E. Plamadeala, and D. Venturelli, arXiv:2006.12731 (2020).
- [49] E. Lieb, T. Schultz, and D. Mattis, Annals of Physics **16**, 407 (1961).
- [50] T. D. Schultz, D. C. Mattis, and E. H. Lieb, Rev. Mod. Phys. **36**, 856 (1964).
- [51] E. Barouch, B. M. McCoy, and M. Dresden, Phys. Rev. A **2**, 1075 (1970).
- [52] T. Ohta, S. Tanaka, I. Danshita, and K. Totsuka, Phys. Rev. B **93**, 165423 (2016).
- [53] D. P. Landau and K. Binder, A guide to Monte Carlo simulations in statistical physics (Cambridge university press, 2014).
- [54] K. M. Nakanishi, K. Mitarai, and K. Fujii, Phys. Rev. Research **1**, 033062 (2019).
- [55] The generalization of the variational principle to more than two orthogonal vectors is similarly shown, which has been used in Ref. [54]